*Graphical Abstract (for review)

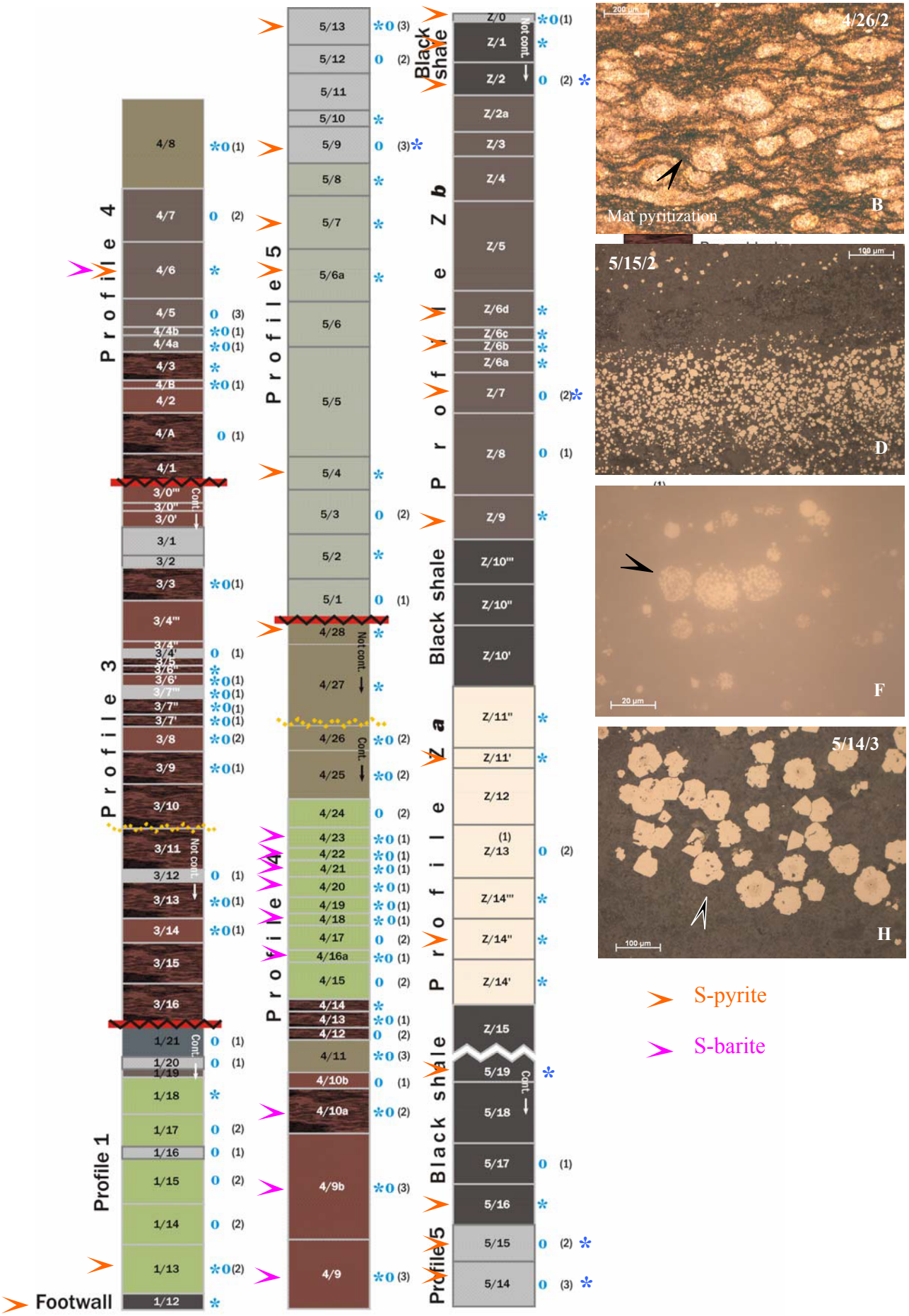

Highlights

- Manganese carbonate microbialites are explicable by a two-step microbial formation model
- Úrkút Mn-carbonate ores bear strong similarities to Molango (Upper Jurassic, Mexico) and Tao Jiang (Middle Ordovician, China).
- Mn, $\delta^{34}S$ values, and trace metals point to the effects of distal hydrothermal fluid sources

Polgári et al. prepared for Gondwana Research (August, 2014)

Sulfur isotopes and correlated chemostratigraphy of Mn-carbonate microbialites (Úrkút, Hungary)

Márta Polgári[1*], Tibor Németh[1], Elemér Pál-Molnár[2], István Futó[3], Tamás Vigh[4] and Stephen J. Mojzsis[1,5*]

[1]Research Center for Astronomy and Geosciences, Geobiomineralization and Astrobiological Research Group, Institute for Geology and Geochemistry, Hungarian Academy of Sciences, Budapest, 1112 Budapest, Budaörsi út. 45, Hungary, e-mail: rodokrozit@gmail.com

[2]Szeged University, Dept. of Mineralogy, Geochemistry and Petrology, Egyetem str. 2-6, 6702 Szeged, Hungary, palm@geo.u-szeged.hu

[3]Institute for Nuclear Research, Hungarian Academy of Sciences, H-4026 Debrecen, Bem tér 18/c, Hungary, futo@atomki.mta.hu

[4]Mangán Ltd, Úrkút, Külterület 1. 8409 Hungary, manganvigh@vnet.hu

[5]Department of Geological Sciences, University of Colorado, 2200 Colorado Avenue, UCB 399, Boulder, Colorado 80309-0399 USA mojzsis@colorado.edu

**corresponding authors:*

rodokrozit@gmail.com, or mojzsis@colorado.edu

Abstract: 240 words **Text:** 4590 words **References:** 35 **Figures:** 6 **Tables:** 1

Supplementary online material

Key words: Jurassic, Manganese carbonate ore, microbial Mn- Fe- oxidation, rhodochrosite, Sulfur isotopes, barite, pyrite

Abstract. Mineral chemistry combined with whole-profile (up section) textural context and sulfur isotopic compositions of associated sedimentary pyrite and barite in the Jurassic (Lias) black shale-hosted manganese carbonate microbialites at Úrkút (central Hungary), can be explained by a two-step microbial formation model (Polgári et al., 2012). Petrogenetic analysis and paleo-environmental reconstructions show that the sedimentary regime of the Úrkút microbialites mostly behaved as an open system during deposition and early diagenesis. Sulfur isotopes and other chemostratigraphic indicators, however, reveal that some horizons reached semi-closed/closed conditions which modulated sedimentation rate and organic matter burial. Barite horizons within Mn-carbonate layers preserve $\delta^{34}S_{VCDT}$ values that average +22.2 ‰, with a maximum at +35.2 ‰. Barite formation most likely occurred under open, or semi-open conditions at diagenesis. The Ba source is attributable to the decomposition of organic matter derived from plankton and other marine organisms, and transformation of biogenic silica. Pyrite-bearing horizons host equant, framboidal and euhedral morphotypes. The distribution of euhedral and framboidal sulfide habits in the Úrkút sedimentary profile is consistent with later diagenetic sulfate reduction zones; more equant types occur at the contact zone of black shale and Mn-carbonate horizons. The microbialites of Úrkút bear strong similarities to analogous ore bodies at Molango (Upper Jurassic, Mexico) and Tao Jiang (Middle Ordovician, China). Manganese supply, $\delta^{34}S$ values, and trace metal contents (Co, Ni, Zn, Cd and As) of the sulfides also point to the effects of distal hydrothermal fluid sources to the system. (**240 words**)

Keywords: manganese carbonate; sulfide; trace elements; microbialite; Jurassic

1. Introduction

Authigenic Fe-sulfides are a common feature of fine grained, organic matter-rich marine sediments throughout the geologic record. They form under anoxic micro-conditions, where reactive organic matter, dissolved sulfate and reactive Fe-minerals co-mingle. As the relative contributions of these different components can vary in different sedimentary environments, their coupling with authigenic Fe-sulfides has long been used as an analytical geochemical facies indicator (e.g. Berner, 1980; Leventhal, 1983; Hámor and Hertelendi, 1991; Hámor, 1994; Vető et al. 1997). Sedimentary Fe-sulfides in such systems are dominantly authigenic phases that form in early diagenesis in the sulfate reduction zone, as such they are a reliable testimony of pore water chemistry (e.g. Sweeney and Kaplan, 1973; Raiswell, 1982; Hudson, 1982). Sulfur isotopic values of authigenic marine Fe-sulfides – sometimes associated with sulfates in carbonates – are commonly used to interrogate the evolution of the marine chemical system, and in particular the long term changes in oceanic sulfate content and a sulfur isotope composition (Holland, 1978).

One such example are accumulations of pyrite-bearing horizons within microbially-mediated laminated Mn-carbonate sediments. Such rocks have been documented in marine sediments spanning the Phanerozoic (e.g. Molango, Mexico – Okita and Shanks, 1988; Moanda, Gabon – Hein et al., 1989; Postmasburg (Kalahari), Southwest Africa – Beukes, 1983; TaoJiang-Minle-Datangpo, China – Fan et al., 1996; Úrkút, Hungary – Polgári et al., 1991, 2012). It is noteworthy that although such sulfidic black-shale-hosted Mn-carbonate ores are economically important and of world-wide occurrence, no examples the formation of such deposits are known for the contemporary ocean. Despite a range of ages these various deposits are broadly similar to one

another, owing to the fact that they are typified by fine grained and "crinkly" organic matter-rich microlaminae generally conformable with bedding typical for microbialites.

At the Úrkút locality in central Hungary, the deposit consists of several (1-3) different meter-scale Mn-carbonate ore beds in a ca. 50 m thick black shale-hosted assemblage. Mineralogical compositions (rhodochrosite, smectite, celadonite, siderite, manganite, goethite, hematite) and isotopic characteristics (strongly depleted $\delta^{13}C$ values) of these ores are also distinctive (reviewed in Okita and Shanks, 1988; Hein et al., 1989; Polgári et al., 1991; Fan et al., 1996). It was argued that such stratiform sediment-hosted Mn-carbonate ore deposits exclusively formed in strictly closed systems within sedimentary basins (Okita and Shanks, 1992; Fan et al., 1996). Most of the black-shale hosted Mn-carbonates are relatively well-preserved (Fan et al., 1996) and have morphological characteristics such as crinkly bedding akin to microbially-induced sedimentary structures; they are microbialites *sensu lato*. Improvements on the general basin models for their deposition, along with the detailed mineralogical and geochemical studies cited above, further bolster the view that Mn-carbonate ores within black shale-hosted deposits in Molango Mexico (Okita el al., 1988); Úrkút, Hungary (Polgári et al., 1991); TaoJiang-Minle-Datangpo-China (Fan et al., 1996) are microbialites.

To explore these relationships further, we undertook a detailed study of the textural and trace element characteristics (e.g. As) of selected pyrite-bearing samples of one of the best examples of a Mn-carbonate deposit, the Mesozoic Úrkút locality in central Hungary (reviewed in Polgári et al., 2003). Here, we report on the geology and geochemistry of the Úrkút Mn-carbonate ores in comparison with other analogous ore deposits, and use these data to construct a model for their genesis. This paper expands on a recently elaborated two step microbial formation model

(Polgári et al., 2012) for the genesis of the Úrkút rocks and elaborates on the formation of self-same ores elsewhere (e.g. TaoJiang, China).

2. Geological setting

The Jurassic (Lias, Toarcian) Úrkút deposit is located in the Transdanubian Range in central Hungary, approximately 150 km west of Budapest (Fig. 1). It is, volumetrically, among the ten largest of its kind in the world. Estimated reserves are about 80 million tons of Mn-carbonate ore that averages ~20 wt.% Mn and 10 wt.% Fe, with an areal extent of tens of square kilometers. The Úrkút deposit occurs within marine sedimentary rocks composed mainly of bioclastic limestone, radiolarian clay marlstone and dark-gray to black shale. Rhodochrosite beds conformably overlie middle Lias (lower Jurassic) cherty limestone. The ore is composed of laminated, alternating gray, green, brown, and black sections composed of mixtures of fine-grained carbonate minerals and clays. The very fine-grained (1–2 µm) rhodochrosite sediments lack either coarse or fine detrital grains (Polgári et al., 2012), and it was argued that ore accumulation took place in a structurally controlled small marine basin in a low-energy and low-temperature depositional environment. The deposit is unmetamorphosed; it was not affected by any significant diagenetic thermal overprinting as shown by oxygen isotope data (Polgári et al., 2012).

The deposit consists of three Mn ore beds (10-, 3-, and 1 m thick) separated by a 20- and 4 m-thick black shale (Fig. 2). The genetic model of Polgári et al. (2012) proposed that two cycles of bacterial activity triggered ore formation: Cycle 1 was an aerobic chemolithoautotrophic cycle that sequestered metal ions (Mn^{2+}, Fe^{2+}) from solution via enzymatic Mn(II) oxidation at the

sediment/water interface. Under this scenario, Mn-oxides were deposited in the sediment pile, serving as a paleoenvironmental indicator of oxic conditions. Cycle 2 was an anaerobic/suboxic heterotrophic bacterial cycle where early diagenetic bacterially mediated Mn(IV) and Mn(III) reduction processes took place via organic matter oxidation and Mn-carbonate mineralization (Polgári et al., 1991, 2012a). The ore sequence is laminated at the millimeter scale reflecting a series of Fe-rich biomats (Polgári et al., 2012b). At the meter scale, the deposit shows color variations where the lower and upper part of the main ore bed is green and the middle part is brown. Towards the middle black shale, the top of the main ore bed is gray.

3. Samples and methods

Powder diffraction on 62 samples (258 subsamples) was performed using a Philips x-ray diffractometer (PW 1710) with carbon monochromator and Cu Kα radiation. Mineral composition was determined on randomly oriented powdered samples by semi-quantitative phase analysis according to the modified method of Bárdossy et al. (1980), using previously defined intensity factors (IGG, HAS, Budapest).

Oriented samples (n=112) were collected along a 917 cm complete section from the footwall to hanging wall from four sections that cross the main ore bed, and one section crossing the upper ore bed (Fig. 2). Bulk and separated lamina sub-samples were examined to determine macroscopic features that cause color and grain-size variations. Petrographic structural-textural studies were made on ninety oriented (bottom and top of sample position) thin sections in transmitted and reflected light mode.

Samples earmarked for sulfur isotopes were chosen based on mineralogy and thin section observations (pyrite and barite occurrence; Fig. 2). The pyrite- and/or barite-bearing samples,

their characterization and the used methods as well as S isotope data reported in the standard delta notation ($\delta^{34}S_{VCDT}$) are summarized in Table 1.

Our $^{34}S/^{32}S$ measurements used the quantitative "Dynamic Flash Combustion" method. Sulfur measurements were made with a Flash Elemental Analyzer (single reactor filled with CuO and copper wires). The chemical trap of magnesium perchlorate removes the water produced in the combustion process. An elemental analyzer NA 1500 NCS Fisons Instruments and Thermo Finnigan ConFlo III system at the Institute for Nuclear Research (HAS, Debrecen, Hungary) combines the high precision of classical multiple sample/standard comparison technique with ease and sensitivity of an on-line interface. The analyte gas (SO_2) from the quantitatively combusted inorganic material was introduced by the ConFlo III system to a Thermo Finnigan DELTA ^{plus} XP isotope ratio mass spectrometer. This continuous flow technique allows automated isotope ratio determination of small gas sample. The S replicate analyses agreed within ± 0.5 ‰.

Quantitative electron microscopy of samples were made on the carbon-coated thin sections (Table 1) using a JEOL Superprobe 733 microprobe equipped with Oxford INCA 2000 energy-dispersive X-ray spectrometer at the Institute of Geology and Geochemistry (HAS, Budapest). Analytical conditions were 20 kV accelerating voltage and 5 nA beam current.

4. Results

4.1. Bulk mineralogy and average chemistry

Bulk and subsample mineral composition of the Mn-carbonate profiles are summarized on Table 1 and Fig 3. Specific descriptions of mineral habit and chemistry are provided below.

The minerals are typically microcrystalline, averaging 1–2 µm in crystal size, with very rare detrital and authigenic mineral grains up to several tens of micrometers in diameter. As previously noted, the bulk mineralogical composition of the Mn-carbonate ore beds is dominated by rhodochrosite (Ca-, Mg-bearing), siderite (second bed), kutnohorite, 10 Å-phyllosilicate (celadonite), smectite (nontronite), goethite, quartz, Ca-apatite (phosphorite) and pyrite, with traces of barite, chlorite, zeolite, feldspar, and manganite. The black shale host consists of quartz, calcite, pyrite, smectite, 10 Å-phyllosilicate (illite, celadonite), goethite, and chlorite, with traces of zeolite, and feldspar. Manganite is the only Mn oxide present in the carbonate-ore bed.

Pyrite occur commonly in the black shale horizons (underlying-b1, middle-b2, overlying-b3, b4), in the first ore sample, in the middle and upper part of the main (i.e. first) ore bed (Polgári, 1993; Polgári et al., 2003). The second and third ore bed is characterized by alternating thin ore and black shale layers, which are macroscopically not distinguisable. Barite occurs in Profile 4 in the middle part of the main ore bed. The average main and trace element composition according to ore types and black shale is summarized in Polgári et al. (2012), which is similar to that calculated here based on mineralogy.

4.2. Pyrite and barite morphology - optical microscopy and SEM-EDS

4.2.1. Pyrite

Euhedral, framboidal and/or equant type pyrite occur rarely in the ore, and when they do it is at the contact of underlying black shale and first ore sample, and top of main Mn carbonate ore bed. Sulfides are frequently found in the black shale horizons (b1, 2, 3, 4; Table 1, Fig. 4).

Euhedral, mainly cubic and/or octahedral pyrites range in size from ~0.5 to 5 µm, and up to 10-30 µm. Framboidal pyrite grains tend to be smaller (0.5-1 µm) and form 30-50 µm clusters that can together are several hundred micrometers across. Equant type pyrite (> 20 µ) are similar to the euhedral and framboidal forms and are often concentrated in layers and lenses.

The underlying black shale (b1) as well as the contact with the main ore bed and b1 (Fig. 5A) is characterized by equant and xenomorphic pyrite. Most of the main Mn-carbonate ores are not pyritiferous, but the upper part of profile 4 (4/24-28) contains pyrite in C_{org}-rich lenses and as pyritized Fe-rich zones that we interpret to have been goethitic biomats (Fig. 4AB). The lower section of profile 5 is more pyritiferous and is rich in euhedral and equant type forms (5/1-7). The top of the main ore bed (5/9, 13-14, grey type ore) is even more pyrite-rich, with massive pyrite layers also occurring there (Fig. 4CD, 5B). Equant type pyrites are the most frequent habit in this sample set (Fig. 4GH). The middle black shale (b2) between the main and second ore beds likewise contains framboidal and euhedral pyrite, and the second bed is characterized by equant and euhedral forms (5/15-19). The b3 and b4 horizons are similar to b2.

4.2.2. Barite

Barite is not visible by conventional optical microscopy and its presence was revealed by x-ray diffraction. As such, analytical electron microscopy was used to investigate the morphology of this mineral. Using this approach, we found that the barite occurs in the lower-middle part of the main ore bed, in profile 4 (4/6, 9, 9b, 10a, 16a, 18, 20, 21, 22, 23, upper green ore type).

Barite is present in the form of (i) disseminated small xenomorphic or semi-euhedral grains (0.5-20 µm, most frequently 1-5 µm, Fig. 5C-G); (ii) in layers among Fe-rich biomat laminae,

surrounded by Ca-rich rhodochrosite and clay bearing matrix (Fig. 5EFG). Barite is always accompanied by quartz (Fig. 5EF). At times, barite vein fillings are found.

4.3. Chemical composition of pyrite and barite

Compositionally, pyrite in our samples is generally pure and homogenous, but in some layers Fe-Co (Ni)-sulfide is also present as well as arsenic-bearing pyrite (b1, upper part of main ore bed).

Barite in these rocks tends to pure Ba-sulfate, but in the brown, upper green and grey type main ore bed and in vein fillings, it is occasionally enriched in Sr.

4.4. Sulfur isotopes

Sulfur Isotope values and distribution in the ore profile are presented in Table 1 and Fig. 2 and 6 for pyrite and barite. These results show that: (i) the underlying black shale (sample 1/12) has $\delta^{34}S$ value –14.7‰; (ii) the lower and middle part of the Mn-carbonate main ore bed (profiles 1, 2, 3, and 4, samples 4/9-6 - 4/23) contain only barite with a S isotope range between + 2.0‰ to + 27.2‰. As an exception, in the first ore sample (1/13) there is pyrite with $\delta^{34}S$ – 8.3‰. In the middle part of the main Mn carbonate ore bed, sample 4/6 contains both pyrite and barite (the only sample which contains both minerals, but in different sublayers), and the pyrite $\delta^{34}S$ value is + 3.0‰, and the barite is + 14.6‰. The samples above it contain only barite (Fig. 2), but just below profile 5, sample 4/28 is also pyritiferous with $\delta^{34}S$ value of + 8.7‰ (pyritized biomat, Fig. 4AB); (iii) The upper part of the main Mn carbonate ore bed (profile 5, samples 5/1/1-5/14/3, Fig. 2) is pyritiferous with a S isotope range from - 7.8 to + 35.2 ‰; (iv) the middle black shale (5/15-5/19) is also pyritiferous with S isotope values between – 24.3 and – 20.3 ‰ (– 10.7 to – 23.4 ‰ was reported for this horizon by Vető et al., 1997); (v) the second Mn carbonate

ore bed is interfingered by black shale and it is difficult to distinguish macroscopically the two facies owing to the fact that the transition is continuous. The second carbonate bed (Z/14-Z/6D) contains pyrite with S isotopes that range from – 0.8 to – 17.9 ‰; (vi) the top black shale (Z/2-Z/1) bed shows has S isotopes between – 31.4 and + 17.1 ‰; (vii) the top-most Mn-carbonate ore layer (Z/0/1) has $\delta^{34}S$ of + 8.4 ‰.

5. Discussion

5.1. Sulfur isotopes and petrogenesis of Úrkút pyrite

The most part of the Úrkút Mn carbonate deposit is pyrite free, as in the ore zones the organic matter alteration took place via microbially mediated Mn(IV,III) reduction and the system did not reach the sulfate reduction zone; it remained suboxic (Polgári et al., 2012a, 2013). The principal pyrite-bearing zones are within the black shales towards the top of the sequence. The distribution of euhedral and framboidal pyrite habits in the ore profile support later diagenetic sulfate reduction zones, whereas equant types are present at the contact zone of underlying b1 and main ore bed defined by the start of the main Mn mineralization period (samples 1/12 and 1/13), the upper gray part of main ore bed towards b2 (termination of main Mn mineralization period; samples 5/9, 13, 14, 15), and the second ore bed (start of second Mn mineralization period; sample Z/0).

Our preferred interpretation of the framboidal pyrite is that they formed via recrystallization of precursor Fe-monosulfide, while the euhedral precipitated directly from solution at low pH. Growth of both framboidal and euhedral types occurs when the diffusive supply is faster than the rate at which the crystal structure can accommodate Fe-S (based on saturation-middle oversaturation; Murowchick and Barnes, 1987). During pyrite formation, the *in situ* conditions

of saturation are supplied from the overlying sediment via reduction to sulfide of a continuous sulfate supply (Fig. 6), as described by Vető et al. (1997). During diagenetic development in sediment pore waters, framboidal pyrite first forms in an open system characterized by considerable enrichment of ^{32}S (strongly negative $\delta^{34}S$ ‰ values; b1,2,3 and 4, Fig. 6). Subsequently, euhedral pyrite forms when the pore volume and the diffusive supply of Fe-S decreases so the system becomes closed. As such, the S isotope values become more enriched in ^{34}S leading to slightly negative or more and more positive $\delta^{34}S$ ‰ values, respectively. The Úrkút sedimentary system behaved as an open system throughout most of its accumulation and early diagenesis. This view is supported by $\delta^{34}S$ values. Some horizons reached semi closed/closed conditions with relatively more positive $\delta^{34}S$ values than contemporaneous Jurassic seawater at around +16 ‰ (Claypool et al., 1980; Table 1, Fig. 6). The Mn carbonates contain enriched values of ^{34}S with an average of +22.2 ‰ (maximum is +35.2 ‰).

Equant type pyrites differ in origin and composition from the framboids and euhedral types described above. Under conditions of extreme oversaturation they precipitate directly from solution and frequently outgrow the pore space, inducing local soft-sediment deformation. Based on these features, the equant type pyrite most probably formed via external pore fluid migration. Sulfur isotope values of the equant type pyrites are also different, they can be very enriched or depleted in ^{32}S depending on the origin of fluid migration. The Úrkút data are strongly negative and moderate positive in $\delta^{34}S$ (-20.3 to +20.8 ‰; Table 1; Fig. 6). Sulfate reduction results in enrichments in ^{32}S and hydrothermal effects tend to drive $\delta^{34}S$ toward heavier values. Perhaps the most important factor to influence the Sulfur isotope signature of sedimentary pyrites is the rate of sediment accumulation because this determines whether the

system is open or closed. In the case of Úrkút, mass balance calculations show that the sedimentation rate was very high (Polgári et al., 2012a).

5.2. S isotope interpretation and genetic considerations of barite

Barite occurs in the lower-middle part of the main ore bed, in profile 4 (upper green ore type), with a $\delta^{34}S$ value between +2.0 and +27.2 ‰ and an average value of +14.2 ‰. Taking into consideration that Jurassic seawater $\delta^{34}S$ was around +16 ‰, it shows that barite formation occurred most probably under a microbially mediated open- or semi-open system during later diagenesis. Barite is a common authigenic constituent of marine sediments (e.g. Rothewell, 1989), in the form of disseminated small grains as in Úrkút, enriched in lenses or layers, and commonly associated with biogenic debris (Cruickshank, 1974; Clark et al., 1990).

Hydrothermal activity can also be proposed for Ba because Fe and Mn contents are very high (Mn-Fe ore), and vein filling Sr-bearing barite bolsters this possibility. Volcanic debris (e.g. ash) alteration as source for Ba can be excluded, as it has been shown that there was no volcanogenic contribution to the deposit (Polgári et al., 2013). A clear association exists, however, between barite and organic matter as previously reported by Boström et al. (1973). The Úrkút barite is also commonly associated with quartz like that noted by Stamatakis and Hein (1993) who proposed that the barite was derived from the diagenesis of biogenic silica. According to the hypothesis of Stamatakis and Hein (1993), the formation of quartz preceded the formation of barite. The source of Ba, therefore, was most likely from the decomposition of organic matter derived from plankton and other organisms, and the diagenesis of biogenic silica. The source of the sulfate ions was from seawater and possibly additional sulfate was produced and utilized in microenvironments from the decomposition of organic matter.

Aqueous barium and sulfate most commonly combined as an abiogenic precipitate within void space generally within organic-rich parts of the sediment. In marine sediments, barite precipitation can be initiated by increasing sulfate or Ba activity or by increasing pH associated with the decay of organic matter (Clark and Mosier, 1989; Maynard and Okita, 1991) and the remains of siliceous plankton such as *Radiolaria* as in Úrkút (Dehairs et al., 1980; Bishop, 1988,; Polgári et al., 2012a). In Tertiary marine sediments, barite mineralization occurs in the opal-CT and clinoptilolite transition, whereas the chalcedony-rich beds are poor in barite (Stamatakis and Hein, 1993). The Lower Jurassic Úrkút deposit contains only authigenic quartz with a small detrital quartz component.

Although most of the main Mn carbonate ore bed is free of pyrite, the barite-bearing zone has a unique distribution. The lower green part of the main ore bed is quartz-rich (30 wt. %; Hahn, 2009; strong diagenetic quartz formation, profile 1, Fig. 2-3), and contains considerable amounts of celadonite reflecting suboxic formation and early diagenetic conditions, but the rhodochrosite and goethite content is low. Owing to the fact that the Mn mineralization was microbially-mediated (Polgári et al., 2012a), and that the goethite is the mineralized remains of microbial mats (Polgári et al., 2012b), the organic matter content in this lower green part of the section is low which explains the absence of barite. The middle brown part of the main ore bed was a dense biomat system that existed under suboxic conditions and aided the anoxic/anaerobic diagenetic formation of nontronite without sulfate reduction and pyrite formation (Polgári et al., 2013, Fig. 2-3). These conditions were probably too anoxic for barite formation, and the silica content is low in this part of the section (2 wt. %; Hahn, 2009). The brown ore section contains the remnants of Mn-oxide “proto ore”, which could not transform

to rhodochrosite via early diagenesis in the absence of sufficient organic material. The barite-bearing upper green part of main ore bed has also low silica content (2 wt. %; Hahn, 2009), but the organic material content was enough to lead to barite mineralization. The formation and diagenetic conditions based on clay mineralogy reflect suboxic conditions (Polgári et al., 2013). The gray top part of main ore bed is strongly pyritiferous, and thus the conditions were not favorable for barite formation.

5.3. Genetic and paleoenvironmental considerations

It is generally accepted that Mn carbonate formation results from suboxic diagenetic reduction of Mn oxide by organic matter (e.g. Okita et al., 1988, Polgári et al. 1991).

Comparing our results with the Molango (Mexico) and TaoJiang (China) Mn-carbonate microbialites reported by Okita and Shanks (1992), data show strong similarities. The Mn-free rocks (black shale zones) in which pyrite is abundant are characterized by depleted δ^{34}S-values typical of microbially-modulate pyrite formation with very similar average data of the three deposits (-24.1 ‰ for Molango; -23.6 ‰ for TaoJiang; and -22.4 ‰ for Úrkút-b2). Manganese-carbonate zones that are relatively poor in pyrite exhibit strong ^{34}S-enrichments. There are also differences between the three deposits. The Molango Mn-carbonate samples (rhodochrosite, Mn-calcite+rhodochrosite and Mn-calcite) have δ^{34}S values that average about -2.3 ‰ with a maximum of +19.7 ‰. The TaoJiang samples have average δ^{34}S values of +1.9 ‰ with a maximum at +24.5 ‰, compared to the average δ^{34}S for Úrkút of +8.8 ‰ with a maximum of +35.2 ‰. The Mn-carbonate ore is also characterized by low total sulfide content, which may be the result of: (i) oxidizing conditions; (ii) influx of sulfate-deficient fresh water; (iii) re-oxidation and loss of metastable sulfides (MnS, FeS; Aller and Rude, 1988); or (iv) closed-system

diagenesis in a system having low sulfate concentrations (Okita and Shanks, 1992). Based on Mn-enrichment processes, we consider oxidizing conditions (scenario i) as the most probable, but the re-oxidation and loss of metastable sulfides (ii) as well as closed-system diagenesis in a system having low sulfate concentrations (iii) cannot be ruled out. Fresh water input can be excluded as all the three deposits were formed in normal marine conditions.

As for what triggered the onset of Mn accumulation, distal hydrothermal discharge, and/or change of Eh conditions are plausible mechanisms.

The gray top part of main ore bed is rich in pyrite, which also accompanies changes to the texture of the ore to coarse euhedral rhodochrosite and equant pyrite (Fig. 5B). We view this as evidence for some external pore fluid migration perhaps from distal hydrothermal influx. This conclusion is also supported by scarce occurrence of Cd-bearing ZnS. Conditions were not favorable for barite formation here, but at some horizons the Sr content of barite, as well as enrichments in Co, Ni and As in sulfides point to the role of occasional hydrothermal input.

6. Conclusions

A whole profile mineralogical, trace element and isotopic study of a microbially-mediated Mn-carbonate ore at the Úrkút locality in central Hungary was undertaken to elucidate its petrogenesis and paleoenvironmental setting. Sulfur isotopes and trace elements were measured in the pyrite-bearing parts of the Úrkút microbialites. These were documented to contain all main pyrite morphotypes, and the distribution of euhedral and framboidal types in the ore profile point to later diagenetic sulfate reduction zones, whereas the equant pyrite types occur at the contact zone of the organic-rich (black shale) and Mn-carbonate ore horizons.

Measured $\delta^{34}S$ values up section show that the Úrkút paleosedimentary system acted as an open system over most of its accumulation time and early diagenesis. Heavier $\delta^{34}S$ values in some zones compared to contemporaneous Jurassic seawater, indicate that only in some horizons reached the semi closed/closed conditions. Based on our analysis, the equant type pyrite most probably formed from external pore fluid migration subsequent to deposition. The most important factor that influenced the Sulfur isotopic composition of sedimentary pyrites is the rate of sediment accumulation, which was high in the Úrkút depositional setting.

Barite occurs in the lower to middle part of the main ore bed, with a $\delta^{34}S$ between +2.0 and +27.2 ‰, the average value is +14.2 ‰. Taking into consideration that the Jurassic seawater $\delta^{34}S$ was around +16 ‰, it means that barite formation most likely happened under microbially mediated open-, or semi-open system during later diagenesis. Barite is a common authigenic constituent of marine sedimentary formations in the form of disseminated small grains as we found it in Úrkút, enriched in lenses or layers, and commonly associated with biogenic debris. Hydrothermal input also played a role because Fe and Mn contents are very high (Mn-Fe ore), and vein filling Sr-bearing barite is present. A clear association exists between barite and organic matter. The source of Ba was dominantly from the decomposition of organic matter derived from plankton and other organisms and the diagenesis of biogenic silica.

Despite the fact that most of the main Mn-carbonate ore bed is pyrite free, the barite-bearing zone has a unique distribution. The lower green part of the main ore bed is rich in quartz, and contains considerable celadonite that we interpret to represent suboxic formation and early diagenetic conditions, but the rhodochrosite and goethite content of these layers is low. The low organic matter content in this lower green part could explain why barite is absent from this

part of the section. The middle brown part of the main ore bed formed from a dense biomat at suboxic to anoxic/anaerobic conditions without sulfate reduction and associated pyrite formation. In addition to the low silica content, these conditions were probably too anoxic for barite formation. Furthermore, the brown ore contains remnants of a Mn-oxide "proto ore", which could not transform to rhodochrosite via early diagenesis in the absence of sufficient organic material. The barite-bearing upper green part of main ore bed likewise has low silica content, but the organic material content was high enough to facilitate barite mineralization. The gray top part of main ore bed is strongly pyritiferous, where the conditions were not favorable for barite formation.

In terms of paleoenvironment, the Mn-carbonate microbialites formed via suboxic diagenetic reduction of Mn-oxide by organic matter. Sub-oxic conditions too oxidizing to support sulfate reduction, were evoked because of the conspicuous scarcity of pyrite and an abundance of oxidized Fe mineralization in the form of goethitic Fe-rich biomats within the Mn-carbonate.

Our results for Úrkút compare well with previous studies of the analogous Molango (Mexico) and TaoJiang (China) localities described in Okita and Shanks (1992).

Cycles of onset and termination of Mn-carbonate production can be related to Mn supply by distal hydrothermal discharge, and/or change in Eh; sulfide crystal habit and trace element contents (Co, Ni, Zn, Cd and As) bolster the view that distal hydrothermal fluids variably affected the nature of deposition in the Úrkút microbialites. **(4590 words)**

Acknowledgments

The study was supported by Hungarian Science Foundation (OTKA-NKTH No. K 68992) to M.P. We thank Alexandra Müller for thin section preparation, and Máté Szabó for SEM-EDS

measurements. A substantial portion of this manuscript was completed while S.J.M. held a Distinguished Research Professorship in Budapest at the Research Center for Astronomy and Earth Sciences of the Hungarian Academy of Sciences.

References

Aller, R. C., Rude, P. D. 1988. Complete oxidation of solid phase sulphides by manganese and bacteria in anoxic marine sediments. Geochim. et Cosmochim. Acta., 52, 751-765.

Berner, R. A. 1980. Early Diagenesis - A Theoretical Approach. Princeton Univ. Press, Princeton, 241 p.

Beukes, N.J., 1983. Palaeoenvironmental setting of iron-formations in the depositional basin of the Transvaal Supergroup, South Africa. In: Trendall, A.F., Morris, R.C. (Eds.), Iron Formation: Facts and Problems. Elsevier, Amsterdam, pp. 131–209.

Bishop, J.K.B. 1988. The barite-opal.organic carbon association in oceanic particulate matter. Nature, 332, 341-343.

Boström, K., Kraemer, T., Gartner, S. 1973. Provenance and accumulation rates of opaline silica Al, Ti, Fe, Mn, Cu, Ni and Co in pelagic sediments. Chem. Geol. 11, 123-148.

Clark, S.H.B. and Mosier, E.L. 1989. Barite nodules in Devonian shale and mudstone of western Virginia: U. S. Geol.Survey Bull. 1880, 30 p.

Clark, S.H.B., Gallagher, M.J., Poole, F.G. 1990. World barite resources: A review of recent production patterns and a genetic association, *in* Minerals, materials and industry: Inst. Mining Metallurgy Cong., 14th, 175-184.

Claypool, G.E., Holser, W.T., Kaplan, I.R., Sakai, H., Zak, I. 1980. The age curves of sulfur and oxygen isotopes in marine sulfate and their mutual interpretation. Chem. Geol., 28, 199-260.

Cruickahank, M.J. 1974. Mineral resources potential of continental margins, *in* Burk, C.A., and Drake, C.L., eds., The geology of continental margins: New York, Springer-Verlag, 965-1000.

Dehairs, F., Chesselet, R., Jedwab, J. 1980. Discrete suspended particles of barite and the barium cycle in the open ocean. Earth Planet. Sci. Letters, 49, 528-550.

Fan, D., Jie, Y., Leiming, Y., Rufan, Z., 1996. The role of microbes in the formation of Mn carbonate during early diagenesis — take the Gaoyan deposit as an example. In: Lianjun, Ye (Ed.), Organism and Organic Matter in the Formation of Mineral Deposits. China Ocean Press, Beijing, pp. 81–101.

Hahn, T. 2009. Mineralogy, cement stratigraphy and geochemistry of manganese ores and host rocks of the Toarcian Úrkút deposit, Hungary. Technical University Bergakademie Freiberg, Germany, MSc dissertation, 84 p.

Hámor, T. and Hertelendi, E. 1991. Relationship between the early diagenetic evolution of sediment and the delta ^{34}S values of sedimentary iron sulfides. Bull. Hung. Geol. Soc., 121, 133-151.

Hámor, T. 1994. The occurrence and morphology of sedimentary pyrite. Acta Geol. Hung., 37, 1-2, 153-181.

Hein, J.R., Bolton, B.R., Nziengui, P., McKirdy, D., Frakes, L., 1989. Chemical, isotopic and lithologic associations within the Moanda Manganese Deposit, Gabon. Abstracts. 28th IGC. Washington DC, pp. 2–47.

Hudson, J.D. 1982. Pyrite in ammonite-bearing shales from the Jurassic of England and Germany. Sedimentology, 29, 639-667.

Leventhal, J.S. 1983. An interpretation of carbon and sulphur relationships in Black Sea sediments as indicators of environments of deposition. Geochim. Cosmochim. Acta, 47, 133-138.

Maynard, J.B. and Okita, P.M. 1991. Bedded barite deposits in the United States, Canada, Germany, and China: Two major types based on tectonic settings. Econ. Geol., 86, 364-376.

Murowchick, J.B. and Barnes, H.L. 1987. Effects of temperature and degree of supersaturation on pyrite morphology. Am. Mineral., 72, 1241-1250.

Okita, P.M. and Shanks, W.C. 1992. Origin of stratiform sediment-hosted manganese carbonate ore deposits: Examples from Molango, Mexico, and TaoJiang, China. Chem. Geol., 99, 139-164.

Okita, P.M., Maynard, J.B., Spiker, E.C., Force, E.R., 1988. Isotopic evidence for organic matter oxidation by manganese reduction in the formation of stratiform manganese carbonate ore. Geochim. Cosmochim. Acta 52, 2679–2685.

Okita, P.M., Shanks III, W.C., 1988. δ^{13}C and δ^{34}S trends in sedimentary manganese deposit, Molango (Mexico) and Taojiang (China): evidence for mineralization in closed system.

Absts., International Association for Sedimentologists. Symposium on Sedimentology Related to Mineral Deposits. Beejing, pp. 188–189.

Polgári, M., Hein, J. R., Tóth, A. L., Pál-Molnár, E., Vigh, T., Bíró, L., Fintor, K., 2012a. Microbial action formed Jurassic Mn-carbonate ore deposit in only a few hundred years (Úrkút, Hungary). Geology 40, 903-906.

Polgári, M., Hein, J.R., Németh, T., Pál-Molnár, E., Vígh, T., 2013. Celadonite and smectite formation in the Úrkút Mn-carbonate ore deposit (Hungary). Sedimentary Geology 294, 157-163.

Polgári, M., Hein, J.R., Vigh, T., Szabó-Drubina, M., Fórizs, I., Bíró, L., Müller, A., Tóth, L. 2012, Microbial processes and the origin of the Úrkút manganese deposit, Hungary. Ore Geology Reviews 47, 87-109

Polgári, M., 1993. Manganese geochemistry reflected by black shale formation and diagenetic processes — model of formation of the carbonatic manganese ore of Úrkút. Special Series of Hungarian Geological Institute. Karpati Publish House, Ushgorod. 211 pp.

Polgári, M., Dobosi, G., Horváth, P., Rálischné Felgenhauer, E., Vigh, T., 2003. As-bearing pyrite at Úrkút and in the Jurassic layers of borehole Iharosberény-I. Bull. Hung. Geol. Surv. 133 (4), 69–475 (in Hungarian with English abstract).

Polgári, M., Okita, P.M., Hein, J.R., 1991. Stable isotope evidence for the origin of the Úrkút manganese ore deposit, Hungary. J. Sed. Pet. 61 (3), 384–393.

Polgári, M., Szabó, Z., Szederkényi, T. (Eds.), 2000. Manganese Ores in Hungary – In Commemoration of Professor Gyula Grasselly – Hungarian Academy of Sciences. Juhász Publishing House, Szeged. 675 pp.

Raiswell, R. 1982. Pyrite texture, isotopic composition and the availability of iron. Am. J. Sci., 282, 1244-1263.

Rothewell, R.G. 1989. Barite, in Rothewell, R.G., ed., Minerals and mineraloids in marine sediments. Amsterdam, Elsevier, 42-46.

Stamatakis, M.G. and Hein, J.R. 1993. Origin of barite in Tertiary marine sedimentary rocks from Lefkas Island, Greece. Econ. Geol., 88, 91-103.

Sweeney, R.E. and Kaplan, I.R. 1973. Diagenetic sulfate reduction in marine sediments. Mar. Chem., 9, 165-174.

Szabó, Z., Grasselly, Gy, 1980. Genesis of manganese oxide ore in the Úrkút basin, Hungary. In: Varentsov, I.M., Grasselly, Gy (Eds.), Geology and Geochemistry of Manganese, Vol. 2. Akadémiai Kiadó, Budapest, pp. 223–236.

Vető, I., Demény, A., Hertelendi, E., Hetényi, M., 1997. Estimation of primary productivity in the Toarcian Tethys — a novel approach based on TOC, reduced sulphur and manganese contents. Palaeogeog. Palaeoclim. Palaeoecol. 132, 355–371.

Figure captions

Fig. 1. Geological sketch map of the Úrkút manganese deposit (after Szabó and Grasselly, 1980). Locality GPS data are: 47°04’55”N; 17°38’40”E

Fig. 2. Geological profile with sample locations of the Úrkút Mn-carbonate deposit (A) and samples (B). (Sampling 2009, Úrkút Mine, Shaft No. III, deep level, +180 m; total No. of samples 112 spanning 917 cm from the base to the top of the three ore layers and the intervening black shale). Key: fragm-fragmented sample; cont.-continuous sampling; not cont.-not continuous sampling; numbers on the stratigraphic columns are sample numbers; * indicates samples for XRD; 0 indicates samples for thin sections (in brackets the number of thin sections, total 90); Profiles 1, 3, 4, 5 are from main ore bed, Profile Za, Zb and Zc are from second ore bed. Patterns show only color varieties and not sedimentary structures.

Fig. 3. Mineral composition (XRD) of Mn-carbonate ore samples and macroscopically separated subsamples normalized to 100% (for sample locations see Fig. 2). The graph was made by coding the estimated quantity of selected minerals (graphics by Gergely Rózsás, Pázmány Péter University). Key: gry-gray; grn-green; brn-brown; blk-black; avg-average.

Fig. 4. Thin section optical microscopy photos. Thin section photos showing Fe-rich biomat structures for different representative samples and magnifications (sample numbers are on the photos), and pyrite. The thickness of the thin sections and the density of biomats are variable **(A, B, C, G** by transmitted light**).** Arrows show representative parts of mineralized filamentous structures, partly pyritized on (A) and (B). **(D, E, F, H)** Reflected light photos of samples, showing euhedral (C, D, E), equant (G, H) and framboidal (F - arrow) pyrite. **(D)** is reflected light photo of (C); **(H)** is reflected light photo of (G). For sample locations see Fig. 2.

Fig. 5. SEM-EDS photos of pyrite and barite in Mn-carbonate ore and black shale (back scattered electron images, for sample localities see Fig. 2). **(A)** Xenomorph Fe-Co-sulfide (P) in fine grained Ca-rhodochrosite (Mn), quartz (Q) and clay (C) matrix, sample 1/13(1); **(B)** Coarse grained equant type pyrite (P), euhedral - semi euhedral Ca-rhodochrosite (Mn) and xenomorf calcite (Ca), sample 5/13(1); **(C)** Fine grained disseminated pure barite (B) in Mn-carbonate ore, sample 4/10a(1), the matrix is quartz (Q), Ca-rhodochrosite (Mn), clay (C) and apatite (A); **(D)** Small barite grains in a lamina, sample 4/10a; the grey scale is the same as on (C); **(E)** Barite grains (B) in the vicinity of early diagenetic quartz (Q) along Fe-rich biomat lamina (Fe), sample 4/18. The matrix is very fine grained Ca-rhodochrosite (Mn) and clay(C) mixture; **(F)** Higher magnification of area signed on (E); **(G)** Barite-rich Ca-rhodochrosite lamina with apatite grain (A) between Fe-rich biomat laminae (Fe) and clay-rich Ca-rhodochrosite matrix. The barite is in connection with quartz (dark-black phases), sample 4/22.

Fig. 6. S isotope distribution of barite and pyrite in the black shale-hosted Mn-carbonate deposit, Úrkút.

Figure 1

Fig. 1.

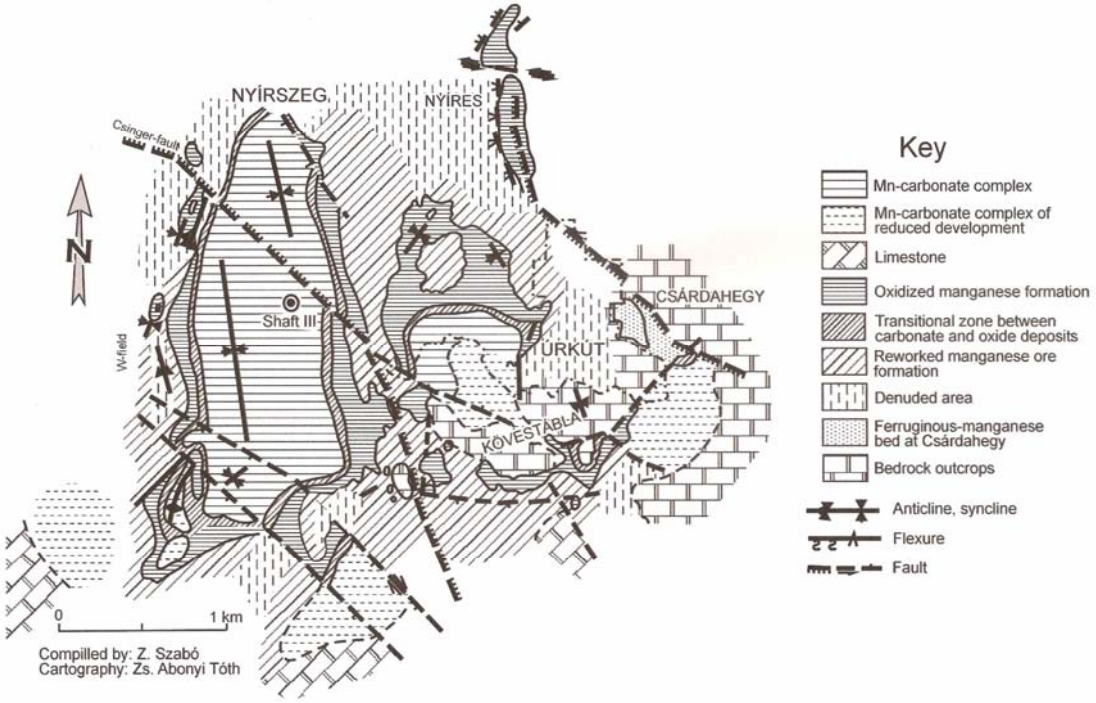

Figure 2

Fig. 2.

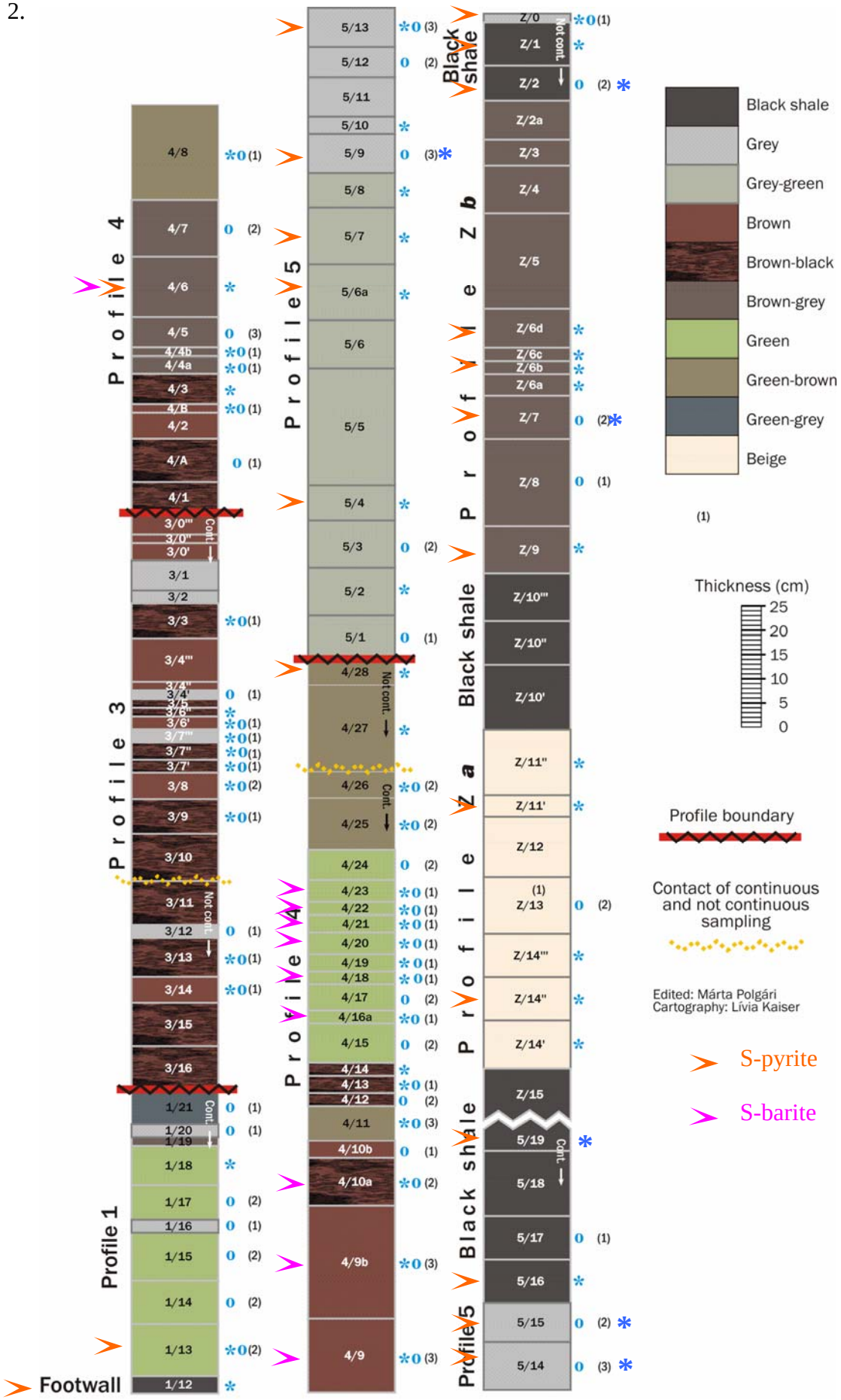

Figure 3

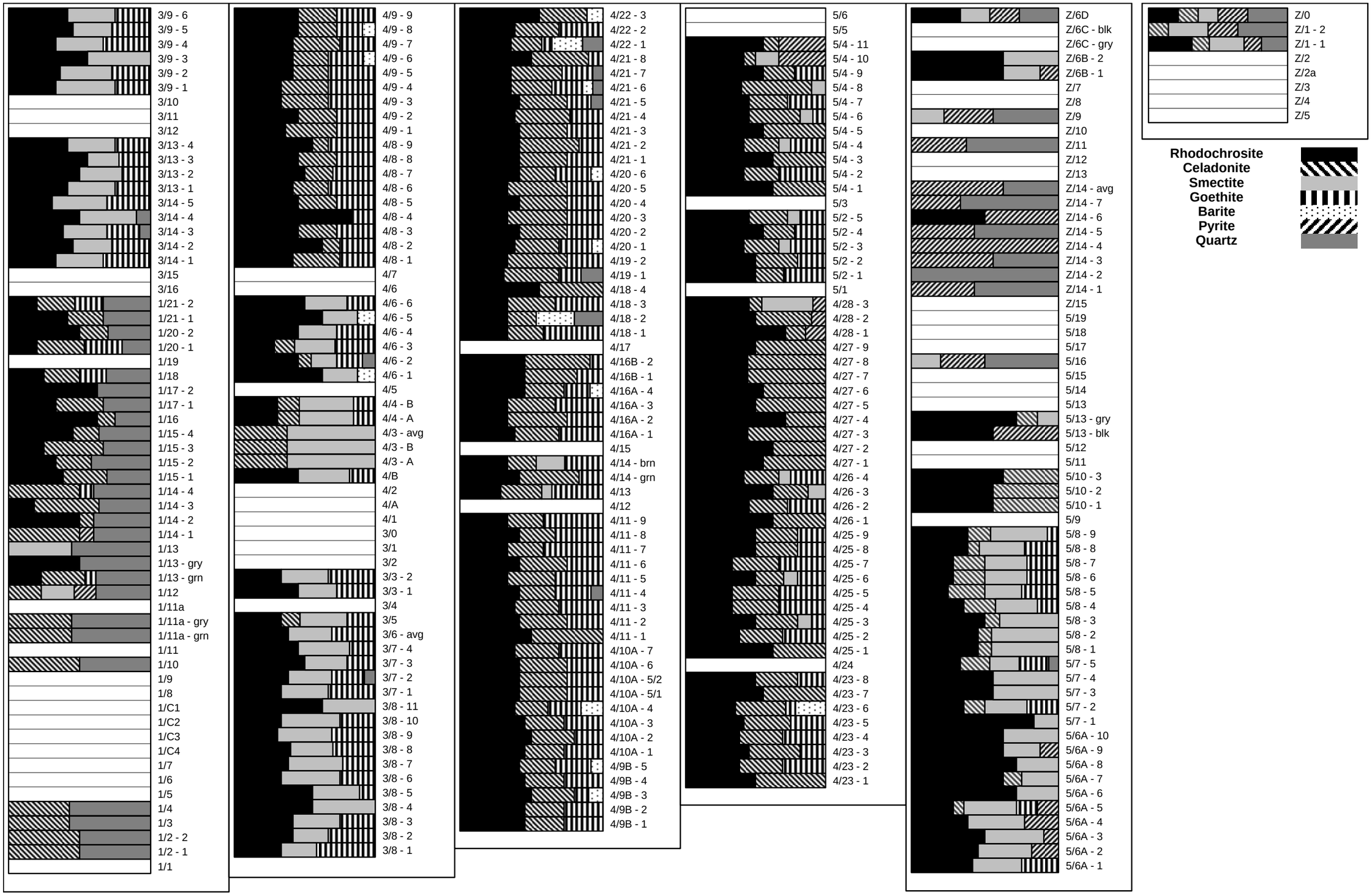
3/9 - 6
3/9 - 5
3/9 - 4
3/9 - 3
3/9 - 2
3/9 - 1
3/10
3/11
3/12
3/13 - 4
3/13 - 3
3/13 - 2
3/13 - 1
3/14 - 5
3/14 - 4
3/14 - 3
3/14 - 2
3/14 - 1
3/15
3/16
1/21 - 2
1/21 - 1
1/20 - 2
1/20 - 1
1/19
1/18
1/17 - 2
1/17 - 1
1/16
1/15 - 4
1/15 - 3
1/15 - 2
1/15 - 1
1/14 - 4
1/14 - 3
1/14 - 2
1/14 - 1
1/13
1/13 - gry
1/13 - grn
1/12
1/11a
1/11a - gry
1/11a - grn
1/11
1/10
1/9
1/8
1/C1
1/C2
1/C3
1/C4
1/7
1/6
1/5
1/4
1/3
1/2 - 2
1/2 - 1
1/1
4/9 - 9
4/9 - 8
4/9 - 7
4/9 - 6
4/9 - 5
4/9 - 4
4/9 - 3
4/9 - 2
4/9 - 1
4/8 - 9
4/8 - 8
4/8 - 7
4/8 - 6
4/8 - 5
4/8 - 4
4/8 - 3
4/8 - 2
4/8 - 1
4/7
4/6
4/6 - 6
4/6 - 5
4/6 - 4
4/6 - 3
4/6 - 2
4/6 - 1
4/5
4/4 - B
4/4 - A
4/3 - avg
4/3 - B
4/3 - A
4/B
4/2
4/A
4/1
3/0
3/1
3/2
3/3 - 2
3/3 - 1
3/4
3/5
3/6 - avg
3/7 - 4
3/7 - 3
3/7 - 2
3/7 - 1
3/8 - 11
3/8 - 10
3/8 - 9
3/8 - 8
3/8 - 7
3/8 - 6
3/8 - 5
3/8 - 4
3/8 - 3
3/8 - 2
3/8 - 1
4/22 - 3
4/22 - 2
4/22 - 1
4/21 - 8
4/21 - 7
4/21 - 6
4/21 - 5
4/21 - 4
4/21 - 3
4/21 - 2
4/21 - 1
4/20 - 6
4/20 - 5
4/20 - 4
4/20 - 3
4/20 - 2
4/20 - 1
4/19 - 2
4/19 - 1
4/18 - 4
4/18 - 3
4/18 - 2
4/18 - 1
4/17
4/16B - 2
4/16B - 1
4/16A - 4
4/16A - 3
4/16A - 2
4/16A - 1
4/15
4/14 - brn
4/14 - grn
4/13
4/12
4/11 - 9
4/11 - 8
4/11 - 7
4/11 - 6
4/11 - 5
4/11 - 4
4/11 - 3
4/11 - 2
4/11 - 1
4/10A - 7
4/10A - 6
4/10A - 5/2
4/10A - 5/1
4/10A - 4
4/10A - 3
4/10A - 2
4/10A - 1
4/9B - 5
4/9B - 4
4/9B - 3
4/9B - 2
4/9B - 1
5/6
5/5
5/4 - 11
5/4 - 10
5/4 - 9
5/4 - 8
5/4 - 7
5/4 - 6
5/4 - 5
5/4 - 4
5/4 - 3
5/4 - 2
5/4 - 1
5/3
5/2 - 5
5/2 - 4
5/2 - 3
5/2 - 2
5/2 - 1
5/1
4/28 - 3
4/28 - 2
4/28 - 1
4/27 - 9
4/27 - 8
4/27 - 7
4/27 - 6
4/27 - 5
4/27 - 4
4/27 - 3
4/27 - 2
4/27 - 1
4/26 - 4
4/26 - 3
4/26 - 2
4/26 - 1
4/25 - 9
4/25 - 8
4/25 - 7
4/25 - 6
4/25 - 5
4/25 - 4
4/25 - 3
4/25 - 2
4/25 - 1
4/24
4/23 - 8
4/23 - 7
4/23 - 6
4/23 - 5
4/23 - 4
4/23 - 3
4/23 - 2
4/23 - 1
Z/6D
Z/6C - blk
Z/6C - gry
Z/6B - 2
Z/6B - 1
Z/7
Z/8
Z/9
Z/10
Z/11
Z/12
Z/13
Z/14 - avg
Z/14 - 7
Z/14 - 6
Z/14 - 5
Z/14 - 4
Z/14 - 3
Z/14 - 2
Z/14 - 1
Z/15
5/19
5/18
5/17
5/16
5/15
5/14
5/13
5/13 - gry
5/13 - blk
5/12
5/11
5/10 - 3
5/10 - 2
5/10 - 1
5/9
5/8 - 9
5/8 - 8
5/8 - 7
5/8 - 6
5/8 - 5
5/8 - 4
5/8 - 3
5/8 - 2
5/8 - 1
5/7 - 5
5/7 - 4
5/7 - 3
5/7 - 2
5/7 - 1
5/6A - 10
5/6A - 9
5/6A - 8
5/6A - 7
5/6A - 6
5/6A - 5
5/6A - 4
5/6A - 3
5/6A - 2
5/6A - 1
Z/0
Z/1 - 2
Z/1 - 1
Z/2
Z/2a
Z/3
Z/4
Z/5
Rhodochrosite
Celadonite
Smectite
Goethite
Barite
Pyrite
Quartz

Figure 4

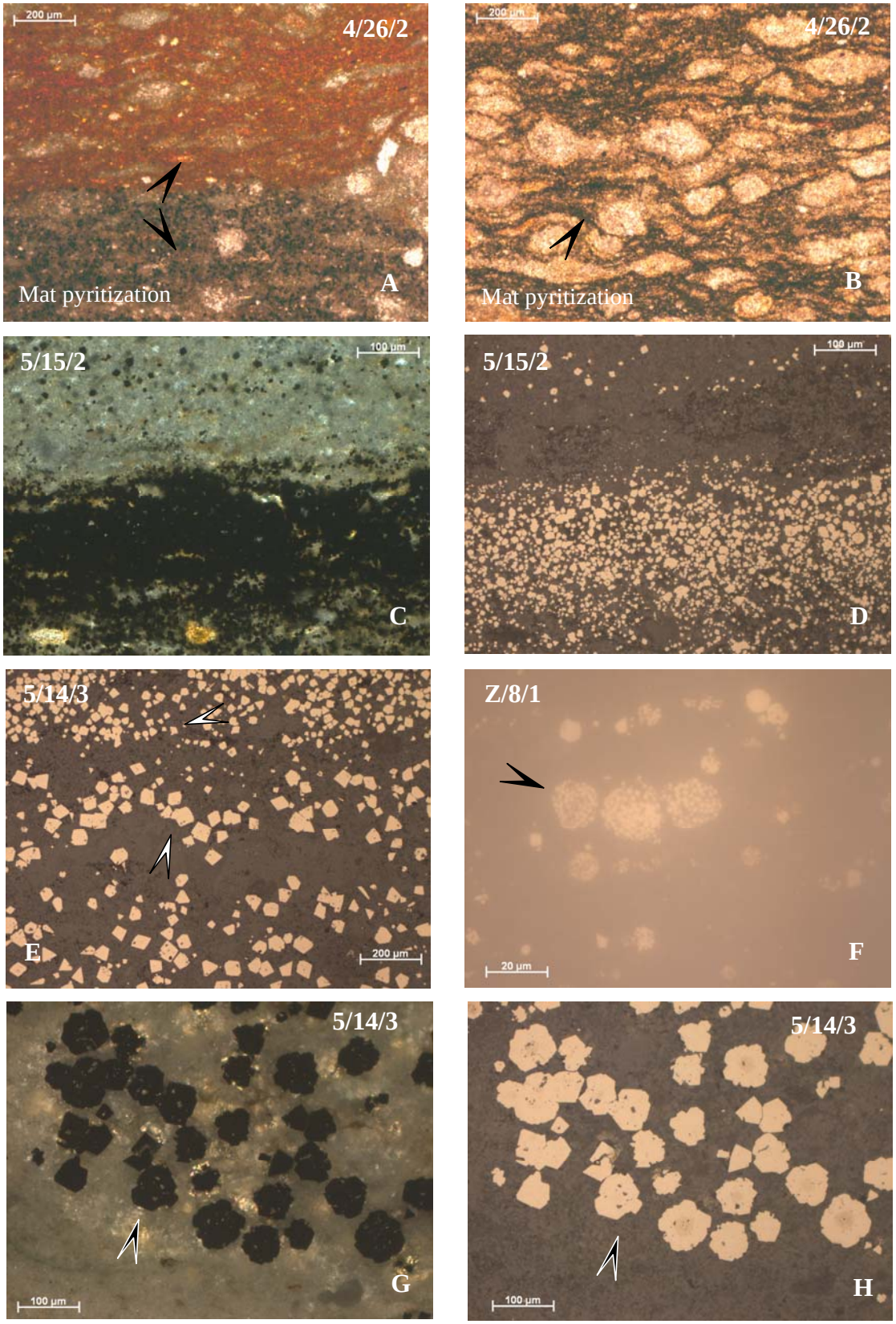
200 µm
4/26/2
Mat pyritization
A
200 µm
4/26/2
Mat pyritization
B
5/15/2
100 µm
C
5/15/2
100 µm
D
5/14/3
E
200 µm
Z/8/1
20 µm
F
5/14/3
100 µm
G
5/14/3
100 µm
H

Figure 5

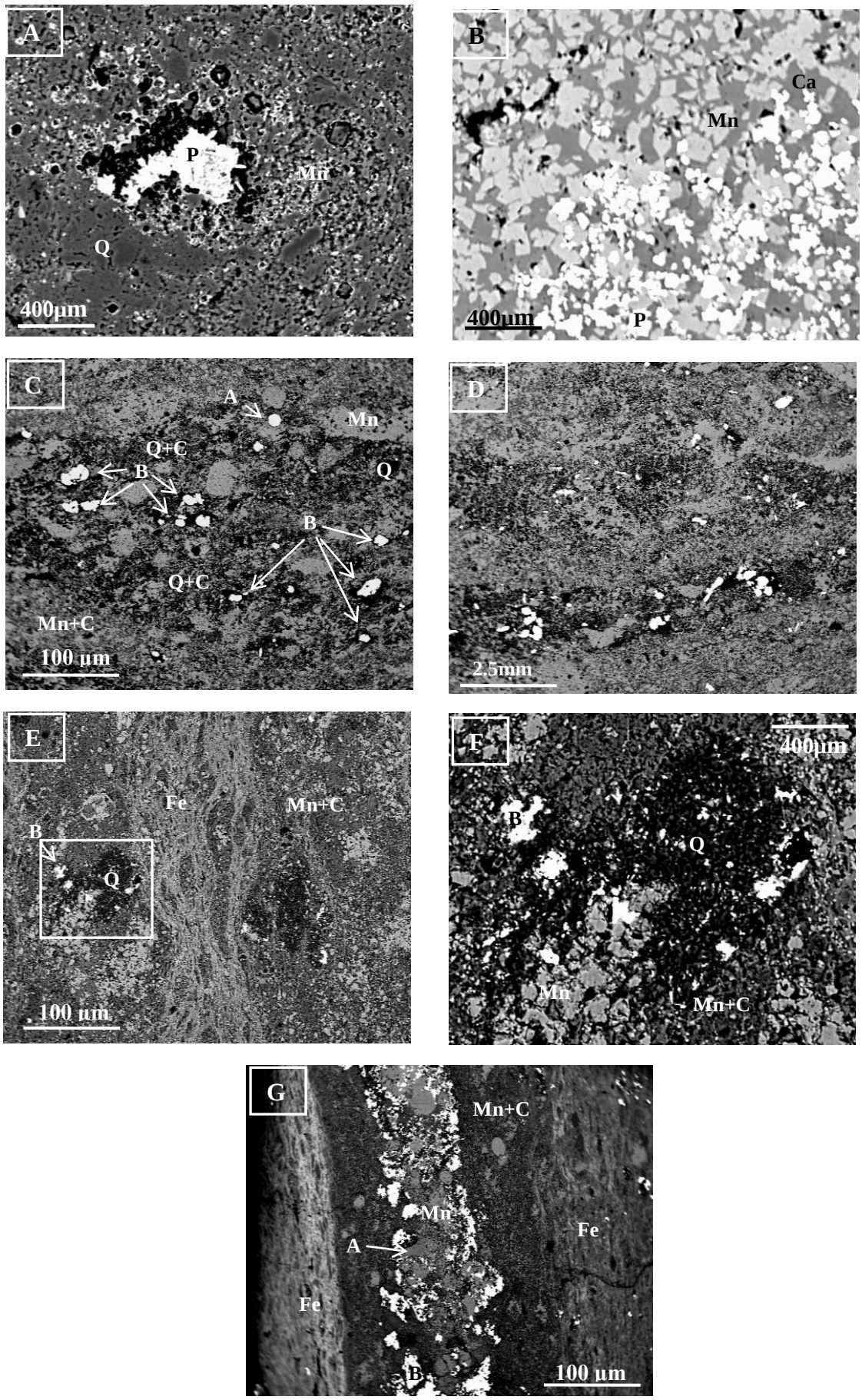
A
P
Mn
Q
400µm
B
Ca
Mn
400µm
P
C
A
Mn
Q+C
B
Q
B
Q+C
Mn+C
100 µm
D
2.5mm
E
Fe
Mn+C
B
Q
100 µm
F
400µm
B
Q
Mn
Mn+C
G
Mn+C
Mn
Fe
A
Fe
B
100 µm

Figure 6

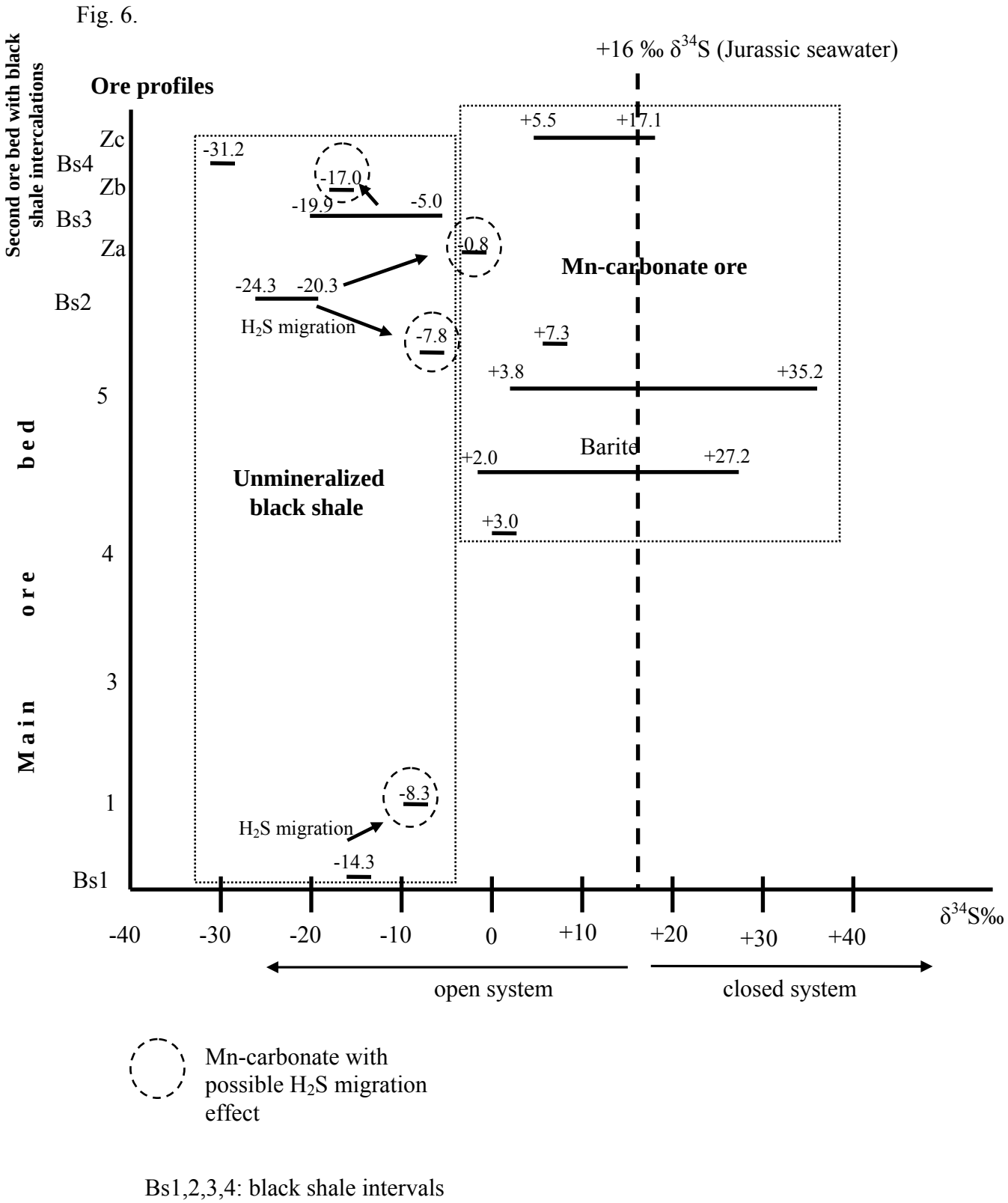

Bs1,2,3,4: black shale intervals

Table

Table 1. Selected samples of ore profile based on pyrite and barite occurrence (XRD and/or thin section study), and S isotope data, morphology and chemistry

System	Bs Effect Pore fluid migration (microbial H_2S)	$\delta^{34}S$ Pyrite (‰)	Sample	$\delta^{34}S$ Barite (‰)	XRD	Thin section	SEM-EDS	Size of pyrite (µm)	Morphology of pyrite	Occurrence Characteristics	Chemistry
open	⟶ Hydr effect?	+8.4	Z/0/1			*	*	~ 50	Eq+E*	Random Sheaf-like sets	
open							*	0.5-1	E	random, dissem*	
open		+5.3	Z/1-2*		*						
open		+17-1	Z/1-1		*						
open		-31.4	Z/2/2		*	*	*	0.5-1 (<50)	F*	random, dissem	
open							*	0.5-1	E	random, disseminated	
open	⟶	-17.0	Z/6D		*						
open	⟶	-17.0	Z/6B-1		*						
open		-5.0	Z/7/2		*			0.5-1 (<50)	F	random	
open								0.5-1	E	Thin and thicker layers (laminae)	
open		-	Z/8/1		-	*	*	0.5-1 (10-20)	F	Disseminated, random	
open							*	0.5-1	E	Along layers (laminae), at some places very rich	
open							*	0.5-1	E	Real pyrite-rich layer (thickness is cca: 500 µm)	
open		-17.4	Z/9		*						
open		-17.9	Z/11		*						
open	⟶	-	Z/13/2		-	*		0.5-1	E	Disseminated + clusters (lenses) in altered Corg-rich parts	
open	⟶	-0.8	Z/14		*						
open		-24.3	5/19		*						
open		-22.5	5/16		*						
open	⟶	-20.3	5/15/2		*	*	*	20-30-4-, 6-	Eq+E+F	Different types are separated by sedimentary horizons, at some zones strong enrichment, thin and thicker layers up to some hundred µm	
open	⟶						*	50 (50-200)	Eq+E+F	Different types are separated by sedimentary horizons, at some zones strong enrichment, thin and thicker layers up to some hundred µm	
open	⟶	+7.3	5/14/3		*	*	*	50-80	Eq+E	In layer equant pyrite (twins?) with core which are homogenous by EDS	Secondary barite veinlets randomly Sr-bearing

open	→						*	0.5-1	E	layers, lenses alternate or disseminated	
open	→						*	10-20	Eq+E	layers, lenses alternate or disseminated	
open	→						*	massive	M*		
open	→	-7.8	5/13/1		*	*	*	massive	M	massive part	ZnS (Cd), Ce (La, Nd, Ca)-phosphate top of main ore bed
open						*	*	10-20	Eq	Disseminated	
Semi-closed/ closed	Hydr effect?	+20.8	5/9/3		*	*	*	10-30	Eq+E	disseminated, frequent	pyrite rich layers also
Semi-closed/ closed							*	0.5-1 (20-30)	F	rare	
Semi-closed/ closed							*	20-50	Eq (6-)	rare, also in layer	finer upstairs
open		+3.8	5/7		*						
open		+16.8	5/6a-9		*	*	*				
Semi-closed/ closed		+22.2	5/6a-4		*	*	*				
Semi-closed/ open		+17.3	5/6a-3		*	*	*				As-bearing pyrite
Semi-closed/ open		+23.5	5/6a-2		*	*	*				
Semi-closed/ closed		+35.2	5/4-11		*						
Semi-closed/ closed		+33.4	5/4-10		*						
		-	5/1/1			*		0.5-1	E	disseminated, and in lenses	
open		+8.7	4/28		*						
			4/26		*	*		1-5?	E	pyritized biomat	
		-	4/24/2			*		1-10	E+M	random in lenses	
			4/23	+26.2	*	*					
			4/22-3	+11.7	*	*	*				
			4/22-1	+27.2	*	*	*				
			4/21-7	+4.5	*	*	*				
			4/21-6	+2.0	*	*	*				
			4/21-5	+18.2	*	*	*				
			4/20-6	+14.8	*	*	*				Sr-traces in barite
			4/20-1	+26.6	*	*	*				
			4/18	+26.5	*	*	*				
			4/16a	+9.6	*	*					
			4/10a	+9.7	*	*	*				
			4/9b-5	+4.0	*	*	*				
			4/9b-3	+8.4	*	*	*				
			4/9-8	+9.1	*	*					
			4/9-6	-10.1	*	*					
			4/6-5	+14.6	*						
open		+3.0	4/6-1		*						
open	→	-8.3	1/13		*	*	*	5-20	Xenomorph pathes		Co-bearing Fe-sulfide
open	Hydr effect?	-14.7	1/12		*	*	*		Eq		As-bearing pyrite

*Sample Note: black shale; Sample note: Mn-carbonate ore; E: euhedral; Eq: equant; F: framboidal; M: massive type pyrite; dissem: disseminated; for sample location see Fig. 2.